RSC Advances

RSC Advances

ARTICLE

Cobalt hydroxide [Co(OH)₂] loaded carbon fiber flexible electrode for high performance supercapacitor

Ajay D Jagadale[a], Guoqing Guan[a,b,]*, Xiao Du[a,c], Xiaogang Hao[c], Xiumin Li [b], Abuliti Abudula[a,b]

Cobalt hydroxide nanoflakes are uniformly loaded on flexible carbon fiber (CF) paper, and provide good electrical connectivity to the current collector for supercapacitor. The unique porous nanostructure offers low ion diffusion and charge transfer resistances in the electrode. The effect of loading mass on electrochemical properties is investigated. The electrode with a mass loading of 2.5 mg/cm² shows the maximum specific capacitance of 386.5 F/g at a current density of 1 mA/cm². Also the same electrode caters good rate capability with energy and power densities of 133.5 Wh/kg and 1769 W/kg, respectively even at higher current density of 10 mA/cm². The electrode reveals a cyclic stability of 92 % over 2000 cycles. This kind of flexible, lightweight electrode could be effectively utilized for the flexible supercapacitor fabrication, especially for wearable electronics.

1. Introduction

Electrochemical capacitors or supercapacitors have been attracted more attentions due to their promising properties of rendering high power and moderate energy densities without compromising cyclic stability. The fabrication of flexible, light weight and high performance supercapacitor is a prime requirement due to its potential application in wearable electronics, mobile phone and computer. Flexible supercapacitor plays an important role in combining high power of conventional capacitors and the high specific energy of batteries[1]. Therefore, fabrication of flexible electrode for supercapacitor is the most focused area of research. Flexible electrode can be prepared using different current collectors, those have been reported are stainless steel fiber (SSF)[2], aligned multi-walled carbon nanotubes (MWCNTs)[3], carbon nanofiber (CNF) paper[4], and so on. Recently, several efforts have been made to prepare the flexible supercapacitor electrode, however some expensive strategies are used which make the obstacle in commercializing such materials[5-7]. Among these materials, flexible carbon microfiber (CF) is a superior current collector owing to its important properties such as low cost, good electric conductivity and good mechanical

integrity[8]. Also as it is a stick network, helps to maintain sufficient electron path[9]. Previously, various CF supported electrodes have been reported for supercapacitor, Bao et al[10] have reported flexible Zn₂SnO₄/MnO₂ core/shell nanocable-carbon microfiber electrode for supercapacitor and showed specific capacitance of 642.4 F/g. Yu et al[11] have prepared reduced graphene oxide sheet wrapped polyaniline nanowire arrays on nitrogen-doped CF cloth for supercapacitor. Recently, Huang et al[12] have prepared a complex electrode made up of nickel–cobalt hydroxide nanosheets coated on NiCo₂O₄ nanowires grown on CF and reported the value of areal capacitance as high as 1.64 F/cm² at 2 mA/cm².

On the other hand, cobalt hydroxide is a frequently reviewed candidate for supercapacitors with superior values of specific capacitance[13,14]. Previously, cobalt hydroxide is reported with various nanostructures including nanoflakes[15], nanosheets [16], nanowires[17], nanoplatelets[18] and nanorods[19]. Among these, cobalt hydroxide with nanoflakes form has unique importance owing to its good electric conductivity, high surface area and good cyclic stability. However, these electrodes are inflexible and could be only utilized for rigid supercapacitor devices. There are very few reports on flexible electrodes formed with hydroxide coating. Warsi et al[20] have made conformal coating of cobalt-nickel layered double hydroxide nanoflakes on CFs for supercapacitor application. Besides, the crystal structure of cobalt hydroxide has been studied widely for supercapacitor application. Basically, it has been reported with two polymorphic phases as α and β-cobalt hydroxides. The α-Co(OH)₂ phase is of hydrotalcite type having water molecules as well as anions like Cl⁻, NO₃⁻ and SO₄²⁻ intercalated in the structure, while the β phase is an ordered staking of neutral Co(OH)₂ layers[21]. An intercalation of ions in the α-Co(OH)₂ could improve the capacitive performance, because their sizes decide the interplanar spacing of basal plane. The enlarged

a. North Japan Research Institute for Sustainable Energy (NJRISE), Hirosaki University, 2-1-3, Matsubara, Aomori 030-0813, Japan
b. Graduate School of Science and Technology, Hirosaki University, 1-Bunkyocho, Hirosaki 036-8560, Japan
c. Department of Chemical Engineering, Taiyuan University of Technology, Taiyuan 030024, P.R. China
*Corresponding author: North Japan Research Institute for Sustainable Energy (NJRISE), Hirosaki University, 2-1-3, Matsubara, Aomori 030-0813, Japan. Tel.: +81 17 762 7756; fax: +81 17 735 5411.E-mail: guan@hirosaki-u.ac.jp .
Electronic Supplementary Information (ESI) available: [details of any supplementary information available should be included here]. See DOI: 10.1039/x0xx00000x

spacing may lead to an enhancement in the transfer rate of proton through interaction between species[22], which could result in the excellent supercapacitive performance.

In the present work, the synergetic effect of pseudocapacitive properties of α-Co(OH)$_2$ nanoflakes and flexible, good electrically conducting CFs is expected to achieve a flexible high performance supercapacitive electrode. As a part of this work, α-Co(OH)$_2$ nanoflakes are uniformly loaded on the CF paper with different mass loadings using potentiodynamic electrodeposition method. The loaded samples are characterized using XRD, SEM and electrochemical analyses. An electrochemical tests of the electrodes have been made through cyclic voltammetry (CV), charging-discharging and electrochemical impedance spectroscopy techniques using three-electrode configuration. An effect of cobalt hydroxide mass loading on electrochemical properties has been systematically investigated.

2. Experimental

2.1 Materials and chemicals

CF paper (Torayca cloth, Toray Industries, Inc.) was used as a flexible substrate material. All chemical reagents were purchased from Wako Chemicals Inc., Japan and used as-received.

2.2. Electrode fabrication

Initially, CF paper was cut into proper dimension. These pieces were cleaned with ethanol and distilled water, and then dried overnight in oven at 50 °C. Further, cobalt hydroxide was loaded onto these paper substrates in 0.1M Co(NO$_3$)$_2$ solution using potentiodynamic electrodeposition method with potential window 0 to −1.3 V vs. Ag/AgCl at 50 mV/s scan rate. The loading masses were varied during potentiodynamic deposition method using potential cycles 20, 30, 40, 50 and 60 as 1.8, 1.9, 2.5, 2.9 and 3.1 mg/cm^2, respectively. The detailed electrodeposition process is explained in our previous article published elsewhere[23]. For the convenience, samples were labeled as CF20, CF30, CF40, CF50 and CF60, respectively. After mass loading, electrodes were rinsed with distilled water and then dried in oven at 50 °C for 1 h.

2.3. Characterization

The morphology and structure of the electrodes were characterized with a scanning electron microscopy (SEM) (Hitachi SU6600, Japan). X-ray diffraction (XRD) patterns were recorded using a diffractometer (XRD 610, Shimadzu, Japan) equipped with a Cu Kα radiation source (λ = 1.5406 Å). The mass loadings were measured by weight difference method using electronic balance.

2.4. Electrochemical measurement

All the electrochemical measurements were performed with a Solartron SI 1280B electrochemical measurement unit. A three-electrode set-up in 1 M LiOH was used for single electrode tests, with gauze platinum and Ag/AgCl as a counter and reference electrodes, respectively.

3. Results and discussion

3.1 SEM

Fig 1 (a) displays photograph of CF paper coated with cobalt hydroxide nanoflakes which clearly shows dark bluish colored cobalt hydroxide layer coated on CF paper. Fig 1 (b) shows schematic diagram of actual mass loading process of cobalt hydroxide onto CF. Fig 1 (c) and (d) show SEM images of bare CF and cobalt hydroxide loaded CF. The size of bare CFs are few micrometers. It was uniformly covered by cobalt hydroxide nanoflakes after mass loading, the inset of Fig 1 (d) shows higher magnification of nanoflakes, estimates the flake thickness in the range of 15–20 nm.

Fig. 1. (a) Photograph of CF paper coated with cobalt hydroxide nanoflakes. (b) Schematic diagram illustrating the loading procedure of cobalt hydroxide on CF. (c) SEM image of bare CF. (d) SEM image of cobalt hydroxide nanoflakes coated on CF. Inset: magnified SEM image of the nanoflakes.

3.2 XRD

The crystal structure and type of polymorph of the cobalt hydroxide were examined by X-ray diffraction measurements. The formation of hexagonal type of cobalt hydroxide nanoflakes with α phase is confirmed, the illustrations for bare CF (a) and CF40 (b) are shown in Fig 2. XRD patterns display noticeable peaks at around 10°, 19°, 33°, 59°, which are assigned to the (003), (006), (012), and (110) planes of the α-Co(OH)$_2$, respectively. The diffraction data matches well with the data reported by Zhu et al for the cobalt hydroxide fabricated by sonication assisted method[24]. The pattern of bare CF sample shows two broad diffraction peaks around 2θ value of 24° and 43°, which may be attributed to the diffraction of (002) and (101) planes of graphite, respectively[25]. The diffraction peak (012) has the typical broad "sawtooth" shape, indicates that the layer stacking in the α-Co(OH)$_2$ might be loose or defective, which could lead to a turbostratic structure[26]. It is a hydrotalcite type of structure with nitrate ions intercalated in the layers. Due to their comparatively smaller sizes they do not impend to OH$^-$ ions during the redox reactions at the interface, which certainly provides healthy environment for the redox reactions at the interface[22].

Fig. 2. XRD patterns of (a) bare CF and (b) CF40 samples.

3.3 Electrochemical measurement

Supercapacitive characteristics of α-Co(OH)$_2$ loaded CF electrodes were performed by CV at various scan rates (Fig. 3). The capacitance mainly arises due to the redox reactions which might be seen from the oxidation and reduction peaks of CV curves. The detail surface faradaic reaction will be as,

$$Co(OH)_2 + OH^- \leftrightarrow CoOOH + H_2O + e^- \qquad (1)$$

ARTICLE

To test the capacitive contribution of CF, we performed CV study for the bare CF electrode, but it was found negligible (figure is not shown). Fig. 3 (a) shows CV curves for CF20, CF30, CF40, CF50 and CF60 electrodes at the scan rate of 5 mV/s in 1M LiOH electrolyte within potential window −0.4 to +0.6 V vs Ag/AgCl. Further, specific capacitance for each electrode was calculated from CV curves using formula[27],

$$C = \frac{1}{mv(V_c - V_a)} \int_{V_a}^{V_c} I(V)dV \qquad (2)$$

where m is the mass of active material in grams, v is the scan rate in V/s, V_a and V_c are the anodic and cathodic potentials in volts, respectively, I(V) is the response current density in ampere and V is the potential. Specific capacitances for each electrode are shown in Fig. 3 (b). The sample CF 40 with a mass loading of 2.5 mg/cm^2 exhibits the maximum specific capacitance of 315.2 F/g at the scan rate of 5 mV/s, which is comparable to the values reported previously for carbon nanofiber/cobalt hydroxide and graphene/cobalt hydroxide composite electrodes[28,29]. The amount of mass loading increases the specific capacitance up to a certain level which may be due to the enhancement in the active mass of the material, however at higher mass loading, relatively active mass of the electrode decreases, so the resultant capacitance decreases with higher extent[30]. Besides, the excess loading mass impedes the kinetics of ion diffusion process during ion

Fig. 3. (a) CV curves of CF20, CF30, CF40, CF50 and CF60 electrodes at the scan rate of 5 mV/s; (b) variation of specific capacitance with mass loading of each electrode; (c) CV curves of CF40 electrode at scan rates of 5, 10, 20, 50 and 100 mV/s; (d) specific capacitances of CF40 electrode at scan rates of 5, 10, 20, 50 and 100 mV/s.

transport in Co(OH)$_2$[31]. Fig 3 (c) depicts CV curves for CF40 electrode at scan rates of 5, 10, 20, 50 and 100 mV/s. The curves exhibit approximately similar shapes and do not change as the scan rate increases from 5 to 100 mV/s, displaying an ideal capacitive behavior with good high-rate capabilities. CV curves for CF20, CF30, CF50 and CF 60 electrodes at various scan rates are shown in Fig. S1 of supporting information. Fig 3 (d) shows specific capacitances at various scan rates for CF40 electrode. As the scan rate increases, the specific capacitance decreases gradually, which can be attributed to the diffusion and migration of electrolytic ions into the active materials at lower scan rates. As scan rate increases up to 100 mV/s, the specific capacitance of CF40 electrode decreases only 43.8% which proves its high rate capability even at higher scan rate. Indeed, at higher scan rate the diffusion effect limits the migration process of electrolytic ions which may cause active surface areas to become inaccessible for the charge storage. The appropriate mass loading of active electrode material is very important aspect to employ these materials for best supercapacitor performance.
In order to evaluate the rate capability of electrodes, galvanostatic charge-discharge was performed at various

current densities within a potential window 0 to +0.5 V vs Ag/AgCl. Fig 4 (a) shows charge-discharge curves for CF20, CF30, CF40, CF50 and CF60 electrodes at the current density of 1 mA/cm^2. The curves are non-linear, display pseudocapacitive behavior with increased discharging time for CF40 electrode. The specific capacitances are also calculated from the discharging branches using formula,

$$C = \frac{I\Delta t}{m\Delta V} \qquad (3)$$

where I is the discharge current, Δt is the discharge time, m is the mass of active material, and ΔV is the potential window (excluding iR drop). The values are observed as 249.2, 283, 386.4, 295.4 and 150 F/g for CF20, CF30, CF40, CF50 and CF60 electrodes at current density of 1 mA/cm^2, respectively. These values are consistent with those calculated from the CV curves.

Fig. 4. (a) Charge discharge curves of CF20, CF30, CF40, CF50 and CF60 electrodes at the current density of 1 A/g; (b) variation of energy and power densities with mass loading of each electrode; (c) Charge discharge curves for CF40 electrode at the current densities of 1, 3, 5, 7 and 10 A/g; (d) Ragone plot for CF40 electrode compared with literature values.

Furthermore, energy and power densities are calculated at the current density of 1 mA/cm^2 for each electrode which is depicted in Fig 4 (b). The energy and power densities have been estimated from the following modified formulae[13],

$$ED = (\Delta E \times I_d \times T_d / 3600)/m \qquad (4)$$

$$PD = \Delta E \times I_d / m \qquad (5)$$

where, I_d is discharge current density (mA/cm^2), T_d is discharge time (hr), m is mass of active material (kg) and ΔE is the potential difference during discharge, excluding iR drop. The CF40 electrode exhibits the maximum energy density of 160 Wh/kg by offering a power delivery of 197.5 W/kg at the current density of 1 mA/cm^2. The power density decreases as the loading mass increases. This is because of the increased internal resistance at higher mass loading. α-Co(OH)$_2$ nanoflakes with a mass loading of 2.5 mg/cm^2 provide low-resistant pathways and short ion-diffusion channels for energy storage and which is expected to achieve high power supercapacitor performance. The present values of energy and power densities are higher than those of recently reported for bare cobalt hydroxide and CF based composite electrodes[32,33]. Fig 4 (c) shows charging discharging curves for CF40 electrode at current densities of 1, 3, 5, 7 and 10 mA/cm^2 (for CF20, CF30, CF50 and CF60 electrodes, see supporting information fig. S2). The CF40 electrode offers energy and power densities of 11.81 W/kg and 1769 W/kg even at a higher current density of 10 mA/cm^2, which is well consistent with the results measured by CV. The results prove the applicability of α-Co(OH)$_2$ loaded CF electrode by offering high power with

excellent energy storage. Fig 4 (c) reflects Ragone plot for CF 40 electrode, the electrode shows high supercapacitive performance with excellent values of energy and power densities, these values in the present case are quite comparable to the recently reported one[34-36]. It is seen that at lower current densities, energy densities are high enough, however, decrease with the increase in the discharge current density. This is attributed to the internal resistance of the electrode. At lower current densities, nanoflakes on the CF surface are wholly utilized for charge storage. In other words, electrolytic ions can easily penetrate into the internal surfaces of the flakes and have access to almost all of the available pores. However, for higher current densities, only outer surfaces of the nanoflakes are utilized which reduce energy density[37]. The excellent supercapacitive performance of CF40 electrode is attributed to the overall high electrical conductivity of the electrode and uniform coating of $Co(OH)_2$ nanoflakes around CF, facilitates rapid electrolytic ions transport.

Fig. 5. (a) Nyquist plots for CF20, CF30, CF40, CF50 and CF60 electrodes within frequency range 20 kHz to 0.1 Hz (inset: magnified image at high frequency region), (b) variation of capacitance retention and cycle number (Inset: charge discharge curves), (c) The electrical equivalent circuit used for fitting impedance spectra

Table 1. The electrical parameters of CF20, CF30, CF40, CF50 and CF60 electrodes estimated from EIS study

Sample /Parameter	R_s	R_{ct}
CF20	2.34	1.36
CF30	2.41	1.43
CF40	2.51	1.66
CF50	2.56	1.73
CF60	3.52	3.50

EIS was utilized to evaluate electrical parameters of α-$Co(OH)_2$ loaded CF electrodes. Fig 5 (a) shows Nyquist plot for CF20, CF30 CF40, CF50 and CF 60 electrodes in the frequency range from 20 kHz to 0.1 Hz. All electrodes show two semicircles in the high frequency region and an inclined line in the low frequency region. The intercept at the real axis in the high-frequency region is related to the internal resistance (R_s), which is a contribution of solution resistance, the intrinsic resistance of cobalt hydroxide and the contact resistance of electrode-electrolyte interface, while R_{ct} results from the diffusion of electrons[37]. The first semicircle is ascribed to the SEI (solid electrolyte interface) resistance and the second semicircle is attributed to the charge transfer resistance (R_{ct}), while the inclined line at lower frequency region represents the diffusion of OH^- ions within the pores of cobalt hydroxide. All electrodes depict the smaller diameters due to their good

electrical conductivities and fast charge transfer reactions. Fig. 5 (c) shows the equivalent circuit fitted for impedance data, the values of R_s and R_{ct} for CF20, CF30, CF40, CF50 and CF 60 electrodes are estimated as shown in Table 1. Table 1 depicts that R_s and R_{ct} values increase with increase in loading mass. Here, CF40 exhibits R_s and R_{ct} values as 2.51 and 1.66 Ω, respectively which are relatively lower than electrodes with higher mass loadings. The CF 40 electrode with α-$Co(OH)_2$ mass loading of 2.5 mg/cm^2 provides lower resistive electronic diffusion and high surface area to achieve excellent supercapacitive performance. In the present study, the mass loading of an appropriate amount 2.5 mg/cm^2 offers low-resistant pathways which might be produced due to short ion-diffusion channels. Furthermore, the cyclic stability of CF40 electrode was tested over 2000 number of charge discharge cycles at the current density of 10 mA/cm^2. Fig 5 (b) shows the variation of capacitance retention over the number of cycles, the stability is observed as 92%. The stability performance in the present case is superior to that of recently reported for cobalt hydroxide based materials[29, 32,38].

Fig 6 (a) Schematic of flexible supercapacitor fabrication, (b) CV curves at bending conditions of 0° and 180° at scan rate of 20 mV/s, (c) Charge-discharge curves at current densities of 0.5, 1 and 3 A/g, (d) Nyquist plot for the supercapacitor within frequency range 10^5 Hz to 0.1 Hz.

To check applicability of electrodes, these electrodes further employed to fabricate flexible solid state supercapacitor. For this, the alkaline PVA/LiOH polymer electrolyte was prepared using a solution casting method. In a typical preparation, PVA (5 g) and $LiOH.H_2O$ (2 g) were mixed and dissolved in 50 mL of water with vigorous stirring for about 4 h at 85 °C. During supercapacitor fabrication, two electrodes with dimension 4cm×4cm were prepared and soaked in the gel like polymer electrolyte for several hours. After soaking, these tow electrodes were stuck together under normal pressure (fig. 6 (a)). Finally the supercapacitor was dried at ambient temperature and used for testing. Flexibility of the supercapacitor was tested by recording CV curves at two different bending conditions. Fig. 6 (b) shows CV curves of supercapacitor at bending conditions of 0° and 180° at scan rate of 20 mV/s. It is clearly seen that the area under curve doesn't change significantly after bending which proves that supercapacitor is highly flexible and does not lose its structural integrity under bending conditions. Fig. 6(c) shows charging/discharging curves of supercapacitor at current densities of 0.5, 1 and 3 A/g. Supercapacitor provides energy and power densities of 4.3 Wh/kg and 424 W/kg at the current density of 3 A/g. Fig. 6 (d) reflects Nyquist plot for the supercapacitor within frequency range 10^5 Hz to 0.1 Hz. The intercept on the real axis is about 1.4 Ω which reveals good conductivity of the electrolyte and low internal resistance of the device.

Conclusions

In summary, α-Co(OH)$_2$ loaded on CF paper with different loading amounts by potentiodynamic electrodeposition method. The effect of mass loading on electrochemical properties is investigated systematically. The CF 40 electrode with a mass loading of 2.5 mg/cm^2 shows the maximum specific capacitance of 386.5 F/g at the current density of 1 mA/cm^2, also the same electrode provides the maximum energy density of 133.5 Wh/kg with power delivery 1769 W/kg at the current density of 10 A/g. The CF 40 electrode has relatively low R$_{ct}$ value, can cater high power performance. The cyclic stability is observed as 92% for the mass loading of 2.5 mg/cm^2. Solid state supercapacitor provides good electrochemical performance with excellent flexibility without losing structural integrity under bending conditions.

Acknowledgement

Notes and references

1 Y.-Y. Horng, Y.-C. Lu, Y.-K. Hsu, C.-C. Chen, L.-C. Chen and K.-H. Chen, *J. Power Sources*, 2010, **195**, 4418-4422.
2 J. S. Kim, S. S. Shin, H. S. Han, L. S. Oh, D. H. Kim, J. H. Kim, K. S. Hong and J. Y. Kim, *ACS Appl. Mater. Interfaces*, 2014, **6**, 268-274.
3 H. Lin, L. Li, J. Ren, Z. Cai, L. Qiu, Z. Yang and H. Peng, *Sci. Rep.*, 2013, **3**, 1353.
4 X. Yan, Z. Tai, J. Chen and Q. Xue, *Nanoscale*, 2011, **3**, 212-216.
5 X. Wang, B. Liu, Q. Wang, W. Song, X. Hou, D. Chen, Y. b. Cheng and G. Shen, *Adv. Mater.*, 2013, **25**, 1479-1486.
6 C. R. DeBlase, K. Hernandez-Burgos, K. E. Silberstein, G. G. Rodríguez-Calero, R. P. Bisbey, H. D. Abruña and W. R. Dichtel, *ACS nano*, 2015, **9**, 3178–3183.
7 C. Zhang, H. Yin, M. Han, Z. Dai, H. Pang, Y. Zheng, Y.-Q. Lan, J. Bao and J. Zhu, *ACS nano*, 2014, **8**, 3761-3770.
8 V. T. Le, H. Kim, A. Ghosh, J. Kim, J. Chang, Q. A. Vu, D. T. Pham, J. H. Lee, S. W. Kim and Y. H. Lee, *ACS nano*, 2013, **7**, 5940-5947.
9 L. Yang, S. Cheng, Y. Ding, X. Zhu, Z. L. Wang and M. Liu, *Nano letters*, 2012, **12**, 321-325.
10 L. Bao, J. Zang and X. Li, *Nano letters*, 2011, **11**, 1215-1220.
11 P. Yu, Y. Li, X. Zhao, L. Wu and Q. Zhang, *Langmuir : the ACS journal of surfaces and colloids*, 2014, **30**, 5306-5313.
12 L. Huang, D. Chen, Y. Ding, S. Feng, Z. L. Wang and M. Liu, *Nano lett.*, 2013, **13**, 3135-3139.
13 A. Jagadale, V. Kumbhar, D. Dhawale and C. Lokhande, *Electrochim. Acta*, 2013, **98**, 32-38.
14 H. B. Li, M. H. Yu, X. H. Lu, P. Liu, Y. Liang, J. Xiao, Y. X. Tong and G. W. Yang, *ACS Appl. Mater. Interfaces*, 2014, **6**, 745-749.
15 M. Li, S. Xu, C. Cherry, Y. Zhu, P. Yang, L. Wang and P. K. Chu, *Electrochim. Acta*, 2014, **149**, 18-27.
16 V. Gupta, T. Kusahara, H. Toyama, S. Gupta and N. Miura, *Electrochem. Commun.*, 2007, **9**, 2315-2319.
17 H. Liu, K. H. Ho, Y. Hu, Q. Ke, L. Mao, Y. Zhang and J. Wang, *Acta Mater.*, 2015, **84**, 20-28.
18 J. Zhou, J. Li, K. Liu, L. Lan, H. Song and X. Chen, *J. Mater. Chem. A*, 2014, **2**, 20706-20713.
19 U. Patil, S. C. Lee, J. Sohn, S. Kulkarni, K. Gurav, J. Kim, J. H. Kim, S. Lee and S. C. Jun, *Electrochim. Acta*, 2014, **129**, 334-342.
20 M. F. Warsi, I. Shakir, M. Shahid, M. Sarfraz, M. Nadeem and Z. A. Gilani, *Electrochim. Acta*, 2014, **135**, 513-518.
21 J. R. Brownson and C. Lévy‐Clément, *Phys. Status Solidi (b)*, 2008, **245**, 1785-1791.
22 Z.-A. Hu, Y.-L. Xie, Y.-X. Wang, L.-J. Xie, G.-R. Fu, X.-Q. Jin, Z.-Y. Zhang, Y.-Y. Yang and H.-Y. Wu, *J. Phys. Chem. C*, 2009, **113**, 12502-12508.
23 A. Jagadale, V. Jamadade, S. Pusawale and C. Lokhande, *Electrochim. Acta*, 2012, **78**, 92-97.
24 Y. Zhu, H. Li, Y. Koltypin and A. Gedanken, *J. Mater. Chem.*, 2002, **12**, 729-733.
25 R. Elazari, G. Salitra, A. Garsuch, A. Panchenko and D. Aurbach, *Adv. Mater.*, 2011, **23**, 5641-5644.
26 Z. Liu, R. Ma, M. Osada, K. Takada and T. Sasaki, *J. Am. Chem. Soc.*, 2005, **127**, 13869-13874.
27 H. Li, M. Yu, F. Wang, P. Liu, Y. Liang, J. Xiao, C. Wang, Y. Tong and G. Yang, *Nat. Commun.*, 2013, **4**, 1894.
28 Z. Tai, J. Lang, X. Yan and Q. Xue, *J. Electrochem. Soc.*, 2012, **159**, A485-A491.
29 Z. Li, J. Wang, L. Niu, J. Sun, P. Gong, W. Hong, L. Ma and S. Yang, *J. Power Sources*, 2014, **245**, 224-231.
30 J. Li, E.-h. Liu, W. Li, X.-y. Meng and S.-t. Tan, *J. Alloy. Compd.*, 2009, **478**, 371-374.
31 L. Hu, W. Chen, X. Xie, N. Liu, Y. Yang, H. Wu, Y. Yao, M. Pasta, H. N. Alshareef and Y. Cui, *ACS nano*, 2011, **5**, 8904-8913.
32 Y. Tang, Y. Liu, S. Yu, S. Mu, S. Xiao, Y. Zhao and F. Gao, *J. Power Sources*, 2014, **256**, 160-169.
33 X. Jiang, Y. Cao, P. Li, J. Wei, K. Wang, D. Wu and H. Zhu, *Mater. Lett.*, 2014, **140**, 43–47.
34 T. Zhai, X. Lu, H. Wang, G. Wang, T. Mathis, T. Liu, C. Li, Y. Tong and Y. Li, *Nano letters*, 2015, **15**, 3189-3194.
35 Y. Tang, Y. Liu, S. Yu, W. Guo, S. Mu, H. Wang, Y. Zhao, L. Hou, Y. Fan and F. Gao, *Electrochimica Acta*, 2015, **161**, 279-289.
36 Y. Bai, W. Wang, R. Wang, J. Sun and L. Gao, *Journal of Materials Chemistry A*, 2015, **3**, 12530-12538.
37 R. Rakhi, W. Chen, D. Cha and H. Alshareef, *Nano Lett.*, 2012, **12**, 2559-2567.
38 X. Cai, S. H. Lim, C. K. Poh, L. Lai, J. Lin and Z. Shen, *J. Power Sources*, 2014, **275**, 298–304.

Fig. 1. (a) Photograph of CF paper coated with cobalt hydroxide nanoflakes. (b) Schematic diagram illustrating the loading procedure of cobalt hydroxide on CF. (c) SEM image of bare CF. (d) SEM image of cobalt hydroxide nanoflakes coated on CF. Inset: magnified SEM image of the nanoflakes.

Fig. 2. XRD patterns of (a) bare CF and (b) CF40 samples.

Fig. 3. (a) CV curves of CF20, CF30, CF40, CF50 and CF60 electrodes at the scan rate of 5 mV/s; (b) variation of specific capacitance with mass loading of each electrode; (c) CV curves of CF40 electrode at scan rates of 5, 10, 20, 50 and 100 mV/s; (d) specific capacitances of CF40 electrode at scan rates of 5, 10, 20, 50 and 100 mV/s.

Fig. 4. (a) Charge discharge curves of CF20, CF30, CF40, CF50 and CF60 electrodes at the current density of 1 A/g; (b) variation of energy and power densities with mass loading of each electrode; (c) Charge discharge curves for CF40 electrode at the current densities of 1, 3, 5, 7 and 10 A/g; (d) Ragone plot for CF40 electrode compared with literature values.

Fig. 5. (a) Nyquist plots for CF20, CF30, CF40, CF50 and CF60 electrodes within frequency range 20 kHz to 0.1 Hz (inset: magnified image at high frequency region), (b) variation of capacitance retention and cycle number (Inset: charge discharge curves), (c) The electrical equivalent circuit used for fitting impedance spectra

Fig. 6 (a) Schematic of flexible supercapacitor fabrication, (b) CV curves at bending conditions of 0° and 180° at scan rate of 20 mV/s, (c) Charge-discharge curves at current densities of 0.5, 1 and 3 A/g, (d) Nyquist plot for the supercapacitor within frequency range 105 Hz to 0.1 Hz.
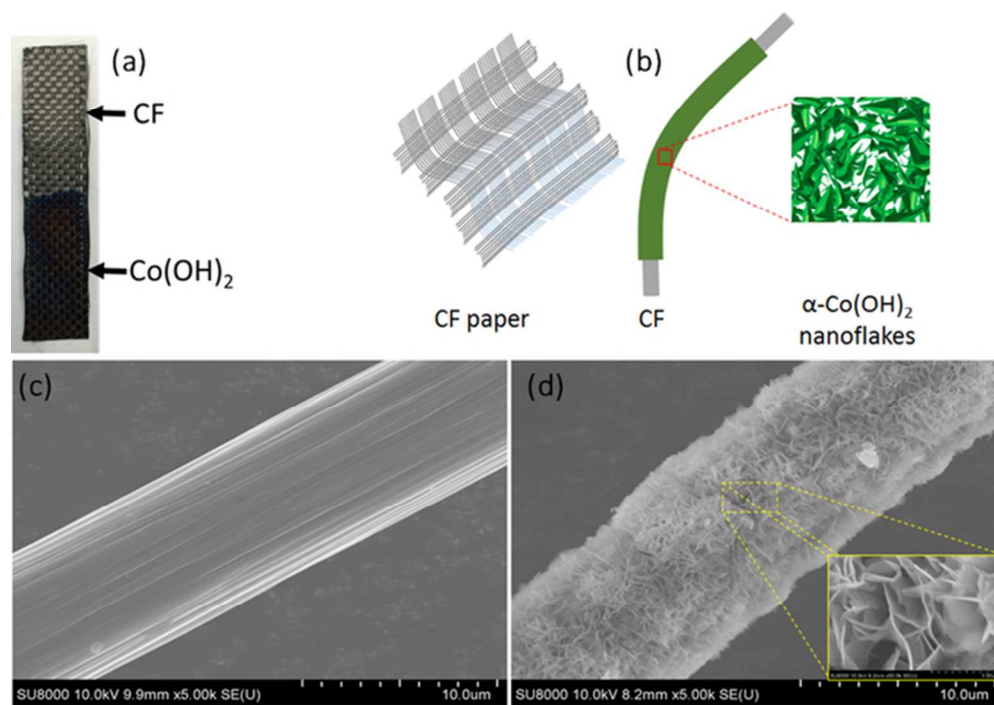
Fig. 1. (a) Photograph of CF paper coated with cobalt hydroxide nanoflakes. (b) Schematic diagram illustrating the loading procedure of cobalt hydroxide on CF. (c) SEM image of bare CF. (d) SEM image of cobalt hydroxide nanoflakes coated on CF. Inset: magnified SEM image of the nanoflakes.
57x40mm (300 x 300 DPI)
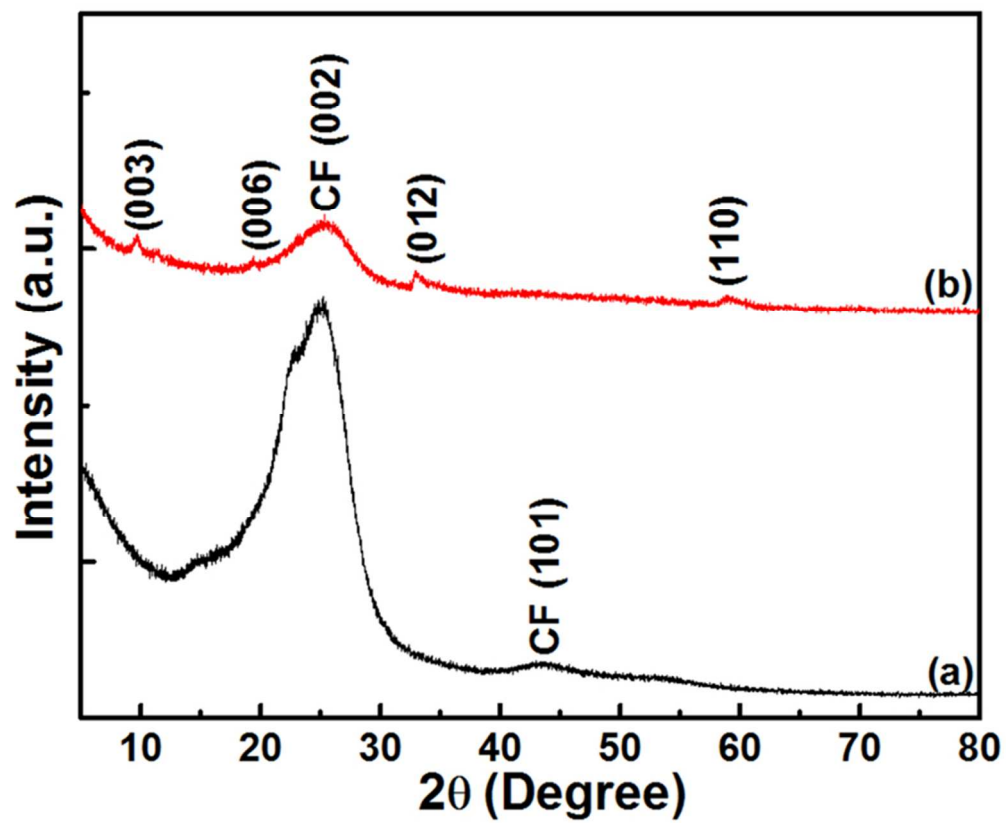
Fig. 2. XRD patterns of (a) bare CF and (b) CF40 samples.
68x55mm (300 x 300 DPI)
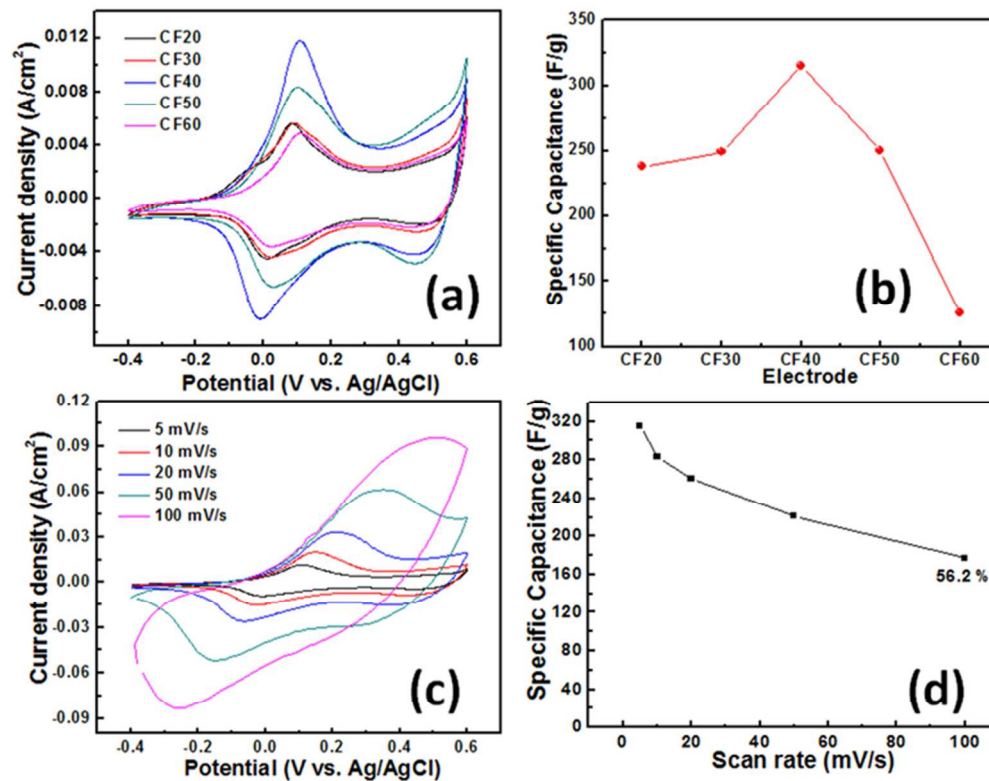
Fig. 3. (a) CV curves of CF20, CF30, CF40, CF50 and CF60 electrodes at the scan rate of 5 mV/s; (b) variation of specific capacitance with mass loading of each electrode; (c) CV curves of CF40 electrode at scan rates of 5, 10, 20, 50 and 100 mV/s; (d) specific capacitances of CF40 electrode at scan rates of 5, 10, 20, 50 and 100 mV/s.
65x52mm (300 x 300 DPI)
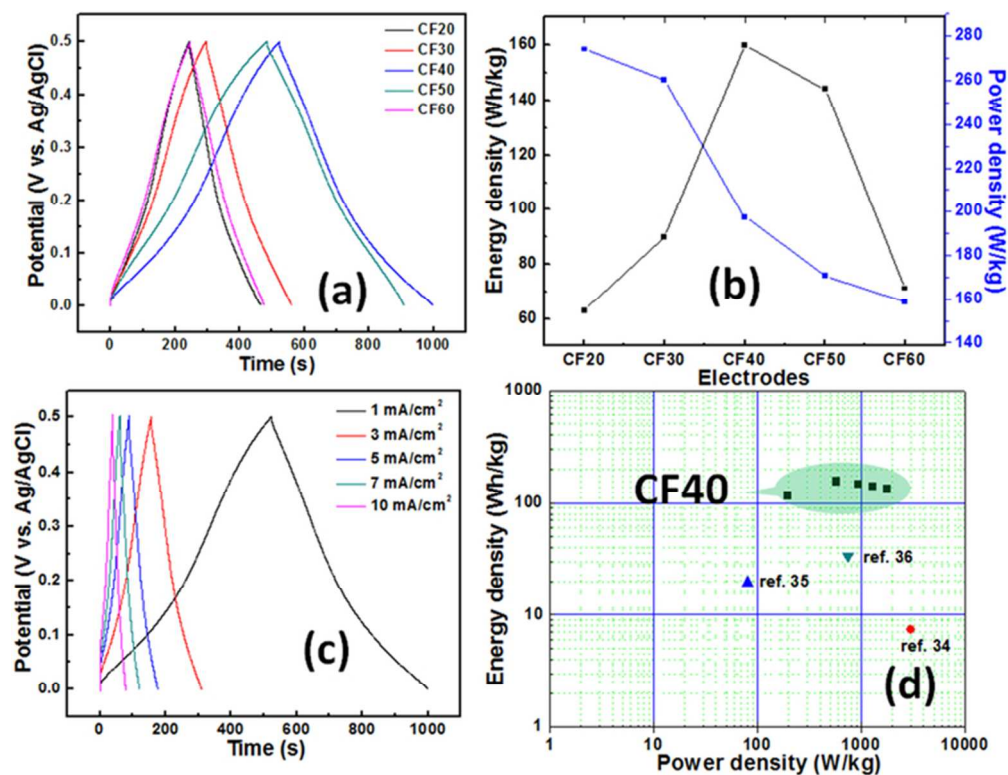
Fig. 4. (a) Charge discharge curves of CF20, CF30, CF40, CF50 and CF60 electrodes at the current density of 1 A/g; (b) variation of energy and power densities with mass loading of each electrode; (c) Charge discharge curves for CF40 electrode at the current densities of 1, 3, 5, 7 and 10 A/g; (d) Ragone plot for CF40 electrode compared with literature values.
63x49mm (300 x 300 DPI)
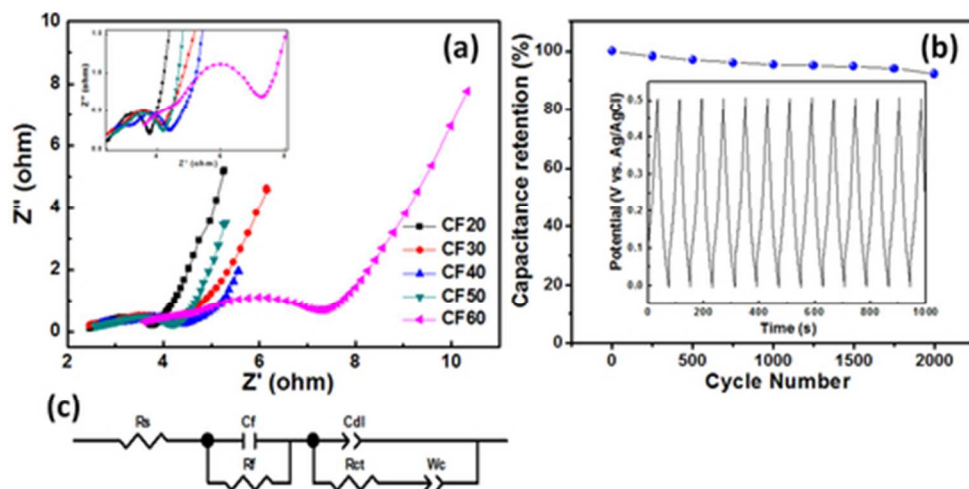
Fig. 5. (a) Nyquist plots for CF20, CF30, CF40, CF50 and CF60 electrodes within frequency range 20 kHz to 0.1 Hz (inset: magnified image at high frequency region), (b) variation of capacitance retention and cycle number (Inset: charge discharge curves), (c) The electrical equivalent circuit used for fitting impedance spectra
41x20mm (300 x 300 DPI)
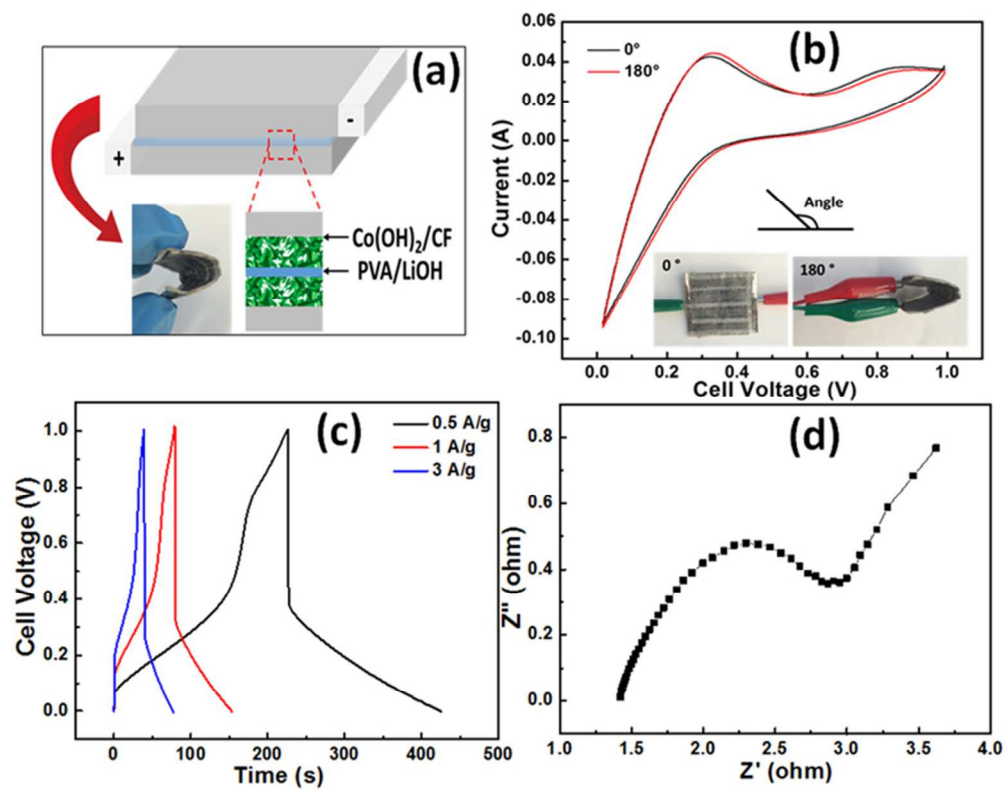
Fig. 6 (a) Schematic of flexible supercapacitor fabrication, (b) CV curves at bending conditions of 0° and 180° at scan rate of 20 mV/s, (c) Charge-discharge curves at current densities of 0.5, 1 and 3 A/g, (d) Nyquist plot for the supercapacitor within frequency range 105 Hz to 0.1 Hz.
64x50mm (300 x 300 DPI)

TOC
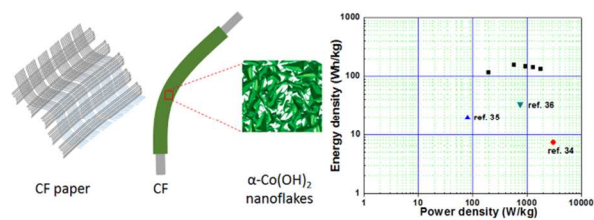
Present work states about successful loading of Co(OH)$_2$ on carbon fiber paper as an electrode for high performance flexible supercapacitor.